Salience network functional connectivity is spatially heterogeneous across sensorimotor cortex in healthy humans

Amy K. Hegarty[a,1], **Moheb S. Yani**[a,1], **Alaa Albishi**[a,b], **Lori A. Michener**[a], **Jason J. Kutch**[a,*]

[a]Division of Biokinesiology and Physical Therapy, University of Southern California, 1540 E. Alcazar Street, CHP 155, Los Angeles, CA 90033, USA

[b]Department of Rehabilitation Sciences-Physical Therapy Division, College of Applied Medical Sciences, King Saud University, Riyadh, Saudi Arabia

Abstract

The salience network is responsive during a range of conditions requiring immediate behavioral responses, including pain processing. Resting-state functional connectivity of the salience network to the sensorimotor cortex is altered in chronic pain. However, little is understood about their fundamental communication in the absence of pain. In this study, we mapped salience network resting-state functional connectivity across sensorimotor cortex in healthy individuals. Using electromyography and task-based functional magnetic resonance imaging (fMRI), we first localized distinct regions-of-interest across sensorimotor cortex in medial (gluteal), intermediate (shoulder), and lateral (hand) areas. We then used resting-state fMRI for two cohorts (primary and replication) of healthy individuals from public repositories to map salience network resting-state functional connectivity across sensorimotor cortex. Both the primary and replication cohorts exhibited significant heterogeneity in salience network resting-state functional connectivity across the sensorimotor regions-of-interest. Using a cortical flatmap to visualize the entire sensorimotor surface, we observed similar heterogeneity in both cohorts. In general, the somatotopic representation of proximal body regions (trunk/face) had higher salience network resting-state functional connectivity compared to distal body regions (upper/lower limbs). We conclude that sensorimotor cortex is spatially heterogeneous in its interaction with the salience network in healthy individuals.

*Corresponding author. kutch@usc.edu (J.J. Kutch).

CRediT authorship contribution statement
Amy K. Hegarty: Conceptualization, Software, Formal analysis, Writing - original draft, Writing - review & editing, Visualization.
Moheb S. Yani: Methodology, Investigation, Data curation, Writing - review & editing. **Alaa Albishi:** Data curation, Writing - review & editing. **Lori A. Michener:** Conceptualization, Funding acquisition, Writing - review & editing. **Jason J. Kutch:** Conceptualization, Supervision, Project administration, Funding acquisition, Writing - original draft, Writing - review & editing.
[1]These authors have equal contribution.

Declaration of Competing Interest
None.

Keywords

Somatotopy; Pain; Motor cortex; Brain mapping; Midcingulo-insular network

1. Introduction

Pain is a subjective experience driven by both bottom-up, and top-down mechanisms where nociceptive inputs are integrated with emotion, affect, mood, and other sensory feedback (Bingel and Tracey, 2008; Tracey and Mantyh, 2007). Integrating such sensory information with autonomic and emotional states is thought to occur within the salience network (SN), a widespread brain network often recognizable even in resting state (Seeley et al., 2007). The interaction between the SN and cortical areas of sensorimotor processing are highly relevant in chronic pain. Previous work in our group has identified changes in resting-state functional connectivity between the salience network (SN) and sensorimotor cortex (S1/M1) specific to the experience of chronic centralized pain (Kutch et al., 2017). These connectivity changes are strongest in specific regions of S1/M1, suggesting resting-state functional connectivity between SN and S1/M1 is somatotopically-dependent. Recent work has validated the presence of somatotopic-specific alterations in SN-S1 resting-state functional connectivity, finding increased connectivity local to the low back region in patients with low back pain (Kim et al., 2019). A widespread network of activation is thought to govern central nervous system response to pain, including activation of SN and sensorimotor system regions (Apkarian et al., 2005; Bingel and Tracey, 2008). Substantial evidence further supports somatotopically-dependent changes in brain activity and structure within S1/M1 associated with chronic pain (Baliki et al., 2012; Kairys et al., 2015; Kutch et al., 2017; Makin et al., 2013; Wu et al., 2013). Such mounting evidence supports a top-down mechanism of chronic pain directly linked to the somatotopy of sensorimotor cortex (Kim et al., 2019; Kutch et al., 2017). Despite the known role of SN and S1/M1 in chronic pain, there is little understanding of the fundamental communication between these regions in healthy individuals. Further, no study has explored the potential relevance of this communication in overall pain perception and development of chronic pain. By mapping the fundamental communication between the SN and S1/M1 in healthy individuals, we hope to explore how the interaction of these brain regions is not only critical for survival but may partially explain features of pain development such as why some body regions are more prone to chronic pain than others.

The role of the SN is thought to broadly provide architecture to filter a stream of sensory stimuli into pertinent and non-pertinent information by redirecting an individual's attention to particular stimuli (Uddin, 2016). The SN is thought to integrate sensory, autonomic, and hedonic information to identify and respond to threats (Seeley et al., 2007). This general function has been inferred from the activation of key SN nodes including anterior insula and anterior cingulate cortex during a wide range of tasks such as empathetic and physical pain, limbic function, error detection, and threat perception (Bastin et al., 2016; Etkin et al., 2006; Seeley et al., 2007; Singer et al., 2004; Wager et al., 2013; Wiech et al., 2010). The integration of sensory information with affective or emotional states within the insula are thought to provide a homeostatic representation of salient stimuli (Craig, 2011). Somatotopic-dependence in S1/M1, secondary sensory cortex and insular cortex suggest the

representation of the body plays a key role in high level processing of salient stimuli both in SN and in its interactions with other cortical areas (Baumgärtner et al., 2010; Ogino et al., 2005; Ruben et al., 2001).

In this study, we explore the underlying interaction between SN and S1/M1 to establish if the relationship between SN and S1/M1 varies across body regions. Given previous findings that the perception of pain is non-uniform across the body (Defrin et al., 2006; Stevens et al., 1974), we hypothesized that healthy individuals exhibit SN-S1/M1 resting-state functional connectivity that is spatially heterogeneous across S1/M1 showing similar heterogeneity in primary motor and primary sensory cortices. This study will provide a foundation to better interpret altered SN-S1/M1 functional connectivity in patients with chronic pain in future studies.

2. Materials and methods

2.1. Summary of study procedures and analyses

Task-based fMRI procedures were used to capture primary sensory (S1) and motor (M1) regions-of-interest (ROI) during the activation of three different muscle groups that were verified to be motorically distinct with electromyographic (EMG) data. SN resting-state functional connectivity within S1/M1 was evaluated in healthy individuals from a publicly available data repository. To understand group trends in SN-S1/M1 resting-state functional connectivity, we used the task-defined ROIs as anchor points of motorically distinct regions of S1/M1 for comparison between body areas. Finally, we evaluated trends in SN-S1/M1 resting-state functional connectivity across the entire S1/M1 cortical surface using a flattened map. SN resting-state functional connectivity results were validated in a second independent cohort of healthy individuals.

2.2. Task-based acquisition and analysis

2.2.1. Participants—A cohort of 20 right hand dominant adults (age: 28 ± 3.4 years, 9 males) participated in a task-based fMRI study. Data collection was completed at the University of Southern California (USC), and all procedures were approved by USC Institutional Review Board. All participants provided their consent to participate. Individuals were excluded if they had contraindications to MRI or had reported history of neurological conditions or chronic pain.

2.2.2. Task-based acquisition—All participants were trained to perform isometric muscle contractions during three movement tasks. Movement tasks were performed supine including: (1) right index finger abduction; (2) right shoulder flexion; (3) bilateral gluteal contraction. During pilot testing, unilateral contractions of the gluteal muscles were difficult for some participants to perform, with substantially higher asymmetric body rotations and head motion in the scanner compared to bilateral contractions. Further, previous work from our laboratory suggests bilateral contractions are associated with bilateral activation in the motor cortex (Yani et al., 2018). Therefore, bilateral gluteal contractions were used to localize the hip ROI. Primary movers for each movement task were identified and muscle activity was collected using electromyography (EMG) during the movement

tasks from each primary mover. The muscles identified as primary movers were the first dorsal interosseous for index finger abduction, anterior deltoid for shoulder flexion, and gluteus maximus for gluteal contraction. EMG signals were collected, amplified, and filtered as previously described (Asavasopon et al., 2014; Rana et al., 2015; Yani et al., 2018). Maximum voluntary isometric contractions (MVIC) were performed for each task. Participants practiced producing a range of contraction intensities as the contraction tasks were replicated in the MRI scanner during task-based scans without EMG. Participants performed repeated 2-s contractions during each movement task to achieve consistent activation at a "low" (L), "medium" (M), and "high" (H) intensity of each primary mover: 15% for L, 30% for M and 45% MVIC for H for the gluteus maximus and first dorsal interosseous muscles, and 30% for L, 45% for M and 60% MVIC for H for the anterior deltoid muscle.

A series of structural and functional MRI scans were then performed using a 3 Tesla scanner (GE Signa Excite) with an eight-channel head coil. Consistent with previously described methods (Yani et al., 2018), we acquired a T1-weighted high-resolution anatomical image from each participant, for the purpose of spatially registering functional images. Next, we collected T2-weighted echo planar image volumes with blood oxygen level-dependent (BOLD) contrast (echo time, 34.5 ms; flip angle, 90°; field of view, 220 mm; pixel size, 3.43 mm) continually every 2.5 s during three movement task imaging runs. Each volume consisted of 37 axial slices (3 mm slice thickness, 0.5 mm interslice gaps) that covered the brain from vertex to cerebellum. Each functional scan was 8 minutes in length consisting of 6 active blocks and 6 rest blocks. During each active block, participants were prompted to perform repetitive sub-maximal contraction at the L, M, and H contraction intensities as described above (block pattern: L-M-H-L-M-H) following visual timing cues within the scanner.

2.2.3. Task-based analysis—All EMG signals were collected during each movement task in a mock MRI scanner with consistent procedures as conducted during the MRI scans. EMG signals were high-pass filtered at 30 Hz (4th order zero-lag Butterworth filter), rectified, and low-pass filtered at 100 Hz (4th order zero-lag Butterworth filter). MVIC trials were processed using the same procedures above, and peak activity was used to normalize each EMG signal during the sub-maximal contraction trials. Finally, each EMG signal was smoothed using a 500 ms moving average window. Task independence was evaluated by comparing EMG activity from the primary mover during the designed movement task against the EMG signals of the reference muscle groups. Peak detection was used to quantify the maximum EMG activity for each muscle contraction. The ratio of peak EMG activity for each reference muscle relative to activity in the primary mover was reported as an average across all participants. EMG activity ratios were determined for each contraction level, each muscle, and across movement tasks. Low ratios of EMG activity between the reference and primary mover muscles would indicate isolation of the primary mover to the designed task.

All fMRI data were preprocessed using FMRIB Expert Analysis Tool (FEAT). Standard processing steps including brain extraction using Brain Extraction Tool (BET) in FMRIB Software Library (FSL), slice timing correction, motion correction using a 12 degree

of freedom model, and spatial smoothing using a Gaussian kernel with full-width half-maximum (FWHM) of 5 mm and nonlinear high-pass temporal filtering (150 s) within FSL were performed for each functional image. Brain regions significantly more active during the muscle contraction blocks of each task (index finger abduction, shoulder flexion, and gluteal contraction) were identified by first comparing the BOLD signal during active and rest blocks using a general linear model (GLM), followed by a group-level mixed-effect (FLAME 1 in FSL) analysis to identify voxels in standard MNI coordinates with significant increases in BOLD signal associated with muscle contraction compared to rest across the cohort of participants (all results were cluster corrected for multiple comparisons with $Z > 2.3$ and $p < 0.05$). The identification of motorically distinct cortical ROIs derived from a task based fMRI approach was previously validated using transcranial magnetic stimulation (Asavasopon et al., 2014; Rana et al., 2015; Yani et al., 2018).

Voxels exhibiting significantly increased activity during muscle contraction were quantified as a z-score based on BOLD signal agreement to the underlying GLM across all study participants. The thresholded z-score images were used to define ROIs representative of each body site (index finger, shoulder, and hip). The tasks were designed to elicit simultaneous voluntary motor and proprioceptive events for each body site, and were therefore used to define both M1 and S1 ROIs. Precentral and postcentral gyri were used as the anatomical landmarks to define the boundaries of the primary motor cortex and primary sensory cortex, respectively (Banker and Tadi, 2019; DiGuiseppi and Tadi, 2019). Voxels significantly activated by the task were separated into voxels within M1 and S1 if the voxel had at least 25% probability of belonging to the precentral gyrus or postcentral gyrus, respectively, defined by the Harvard-Oxford atlas (Makris et al., 2006). For unilateral movement tasks (index finger abduction and shoulder flexion) significant voxels in ipsilateral hemisphere were not considered. The center of each active area was quantified using the three dimensional center of mass of each activity cluster. This resulted in 6 ROIs, one region in M1 and S1 for each movement task. Volumetric ROIs were then built as spherical regions with a radius of 6 mm placed on the active cluster center for each task.

The influence of inter-individual variability in the development of task-defined ROIs were explored by calculating participant specific task-defined ROI centers. Participant specific activity clusters were derived from statistical maps of each voluntary contraction task. First level statistical maps representing the strength of agreement between the BOLD signal and the event related hemodynamic response function were thresholded using a cluster corrected approach for multiple comparisons ($Z > 2.3$ and $p < 0.05$). Primary motor and primary sensory activity cluster centers were defined as the center of gravity for clusters in precentral and postcentral gyrus, respectively.

2.3. Resting-state fMRI data and analysis

2.3.1. Participants and data—Resting-state fMRI (rs-fMRI) images from two publicly available repositories of healthy individuals were included for analysis: the 1000 Functional Connectome Project (http://www.nitrc.org/ir, Biswal et al., 2010) and the Multidisciplinary Approach to the Study of Pelvic Pain (MAPP) Research Network (https://www.niddkrepository.org, Alger et al., 2016). To generate the *primary cohort*, participants

were included from the 1000 Functional Connectome Project. Data from a total of 1288 participants from 33 unique data collection sites were examined. An initial data search constrained the participant dataset to rs-fMRI acquisition parameters consistent with MAPP (3 Tesla scanner with repetition time (TR) = 2 s) resulting in 634 possible participants. From those, 489 participants with known age and sex were selected and preprocessing was performed (see below). The dataset was then further constrained to meet strict head-motion criteria; peak framewise displacement less than 0.3 mm (Drysdale et al., 2017), resulting in 217 possible participants. Finally the cohort's mean age and sex proportion was matched to the task-based fMRI group by iteratively removing participants with the maximum deviation from the desired mean age, resulting in a total of 154 participants (age: 27 ± 11 years, 69 Males, 9 sites) in the final primary cohort. This large healthy control repository afforded us the advantage to carefully control for head motion confounds. However, given our previous findings of altered SN-S1/M1 resting-state functional connectivity in chronic pain, we were concerned that heterogeneity we may observe in the primary cohort could be driven by a participant's unassessed pain history within these otherwise healthy individuals. To address this concern, we generated a *replication cohort* of healthy participants who were verifiably pain free from the MAPP study. The MAPP dataset contained 124 healthy controls, each assessed for pain in the last 2 weeks on a 45-location body map of pain (Brief Pain Inventory) (Kutch et al., 2017; Kutch et al., 2015). Eighty-two participants were identified after excluding those who reported pain at any body location. Finally, samples were removed if peak framewise displacement during the rs-fMRI scan exceeded 2 mm, previously recommended as an adequate threshold for rs-fMRI data (Poldrack et al., 2011). Despite the potential of additional noise compared to the conservative threshold for head motion identified above, this threshold was chosen to maximize the participant pool of pain-free controls for analysis. These selection criteria resulted in a sample size of 66 pain free healthy controls (age: 36.0 ± 11.3, 42 males, 5 sites).

2.3.2.   Resting-state fMRI analysis—rs-fMRI preprocessing was performed using FSL FEAT where functional images were first skull extracted using brain extraction tool (BET), motion corrected, and spatially smoothed using a Gaussian kernel of full-width half-maximum of 5 mm and nonlinear high-pass temporal filtering (150 s). The first four volumes were removed to allow for signal stabilization. All fMRI images were then transformed into 3mm MNI standard coordinates to enable voxel by voxel comparisons across participants. A data-driven analysis of resting-state functional connectivity was completed using Independent Component Analysis (ICA). Group average analysis was completed within the study population by concatenating volume-by-volume all rs-fMRI images and performing ICA on the concatenated images using FSL's MELODIC tool (Woolrich et al., 2009). The analysis was constrained to 20 components to limit identification of sub-components (Kutch et al., 2017). The set of spatial maps from the group analysis was used to generate subject-specific versions of the spatial maps, and associated timeseries, using dual regression with variance normalization (Beckmann et al., 2009; Filippini et al., 2009).

2.3.3.   Post-processing and statistical analysis—The SN was identified from the 20 independent component spatial maps by computing the best fit between each independent

component map and a template of the SN previously published (Laird et al., 2011). The SN was identified separately for both the primary and replication cohort. SN-S1/M1 resting-state functional connectivity measure was reported as a normalized z-score, quantified as the strength of SN signal divided by the unassigned error in each voxel's BOLD signal. SN resting-state functional connectivity across S1/M1 was mapped using an ROI analysis for both the primary and replication cohort as follows. SN-S1/M1 resting-state functional connectivity for each participant was quantified from dual regression generated spatial maps. SN-S1/M1 connectivity was averaged across all voxels within the each of the six spherical ROIs (index finger, shoulder, and hip), and separately compared in M1 and S1 ROIs (3 in M1, 3 in S1) using a linear mixed effect model. A single mixed effect model was used to statistically contrast SN-S1/M1 resting-state functional connectivity for the 3 primary motor ROIs, where body site (factor levels: index finger, shoulder, hip), participant age, sex (factor levels: male, female) and imaging site (factor levels: site 1, site 2, …, 9) were fixed effects, and a random intercept was included for each participant. All categorical variables were modeled using dummy variable reference coding. A congruous mixed-effect model was used to statistically contrast SN-S1/M1 resting-state functional connectivity for the 3 primary sensory ROIs with the same design described above. Confounds including scanner site, age and sex have all been previously shown to affect functional connectivity findings (Damoiseaux et al., 2007; Ingalhalikar et al., 2014; Kilpatrick et al., 2006; Noble et al., 2017), and were therefore controlled in this study as confounds of no interest within the linear mixed effects model. Pairwise differences between ROIs were statistically tested using the linear model coefficient t-test, corrected for multiple comparisons using Bonferroni corrections ($a = 0.05$).

SN-S1/M1 resting-state functional connectivity was mapped from the fiducial cortical surface (surface half way between pial and white matter boundary) using the group average SN spatial map to visualize results on a flattened map of the entire cortex. The fiducial cortical surface was flattened by inflating and cutting the cortical surface at 5 locations along the medial hemisphere surface, taking special care not to cut portions of the precentral or postcentral gyrus. Cuts were used to limit distortion of the cortical surface during flattening (Gao et al., 2015). M1 and S1 boundaries were manually traced on the cortical surface using the Harvard–Oxford atlas with 25% or greater probability map for region identification. Finally, SN-S1/M1 resting-state functional connectivity was expressed on the cortical flatmap as a function of distance to the major hubs within SN, the anterior insula and anterior cingulate. Peak activity within the left anterior insula and left anterior cingulate were assessed as the maximum z-score within the SN map in the anterior insula and anterior cingulate in the left hemisphere. SN-S1/M1 resting-state functional connectivity was then assessed as a function of geodesic distance to each SN hub.

3.   Results

3.1.   Head motion in fMRI scans

All fMRI scans included in this study were well controlled to limit head motion artifacts. Framewise displacement in task-based scans was low with 99% of all image frames having less than 2 mm of displacement, with average peak framewise displacement of

1.3 mm during the shoulder flexion task, 0.6 mm during the index finger task, 1.1 mm during the gluteal contraction task (Supplemental Fig. 1). Resting-state images were also quality controlled to limit motion artifacts and maximize statistical power for both cohorts. Head motion was strictly controlled within the primary cohort with maximum framewise displacement equal to 0.3 mm. Head motion was also closely evaluated in the replication cohort where the maximum framewise displacement was limited to 2 mm, and 92% of all image frames had less than 0.3 mm displacement. We chose to use a stringent motion threshold in the primary cohort to ensure the findings were not influenced by head motion artifacts. Within the 1000 Functional Connectome repository, there were abundant high quality resting-state scans allowing us to use an especially stringent motion threshold without the inclusion of censoring or other motion artifact reduction techniques, which each present a unique challenge and potential pitfalls in resting-state analysis (Caballero-Gaudes and Reynolds, 2017). While this motion threshold was a good starting point, the threshold was unfeasibly stringent for data collected in a single study, as was the case for the replication cohort. Therefore a second, less stringent, motion threshold was adopted to maximize the available participant set within the replication cohort. Further description of overall head motion characteristics of this study are reported in Supplementary Fig. 1.

3.2. Regions-of-interest in primary sensorimotor cortex

EMG data recorded during the three movement tasks showed largely independent muscle contraction patterns for the primary movers of each task (Fig. 1 (A)). During the index finger abduction task, non-primary mover EMG activity was less than 1.3% of primary muscle activity. During the shoulder flexion task, non-primary mover EMG activity was less than 15% of primary muscle activity, likely higher due to the increased need for core stabilization, but still a relatively low percentage. During the gluteal contraction task, non-primary mover EMG activity was less than 3.4% of primary muscle activity.

Clusters of significant brain activity were present in both precentral and postcentral gyri for all three movement tasks (Fig. 1 (B)). The center of significant brain activity during the movement task was identified in lateral S1/M1 for the index finger, in mid S1/M1 for the shoulder and in medial S1/M1 for the hip (Table 1, Fig. 1 (C)). Group derived task-based ROIs (Table 1) well represented the mean response across all study participants. Similarly, while inter-individual variability was evident in participant-level activity cluster centers, clear delineations are present between activity centers for the index finger task, compared to the shoulder task, and compared to the gluteal task (Supplementary Fig. 2). The group derived task-based ROIs were used as anchor points to explore SN-S1/M1 resting-state functional connectivity.

3.3. Resting state independent component analysis

The SN spatial map was identified in both cohorts with high network strength in bilateral anterior insula, anterior cingulate cortex, secondary sensory cortex (S2), thalamus, and amygdala (Fig. 2 (A)).

3.4.   Region of interest analysis

Significant heterogeneity of SN resting-state functional connectivity across S1/M1 in both the primary and replication cohorts were observed both in M1 and S1 ROIs (Fig. 2 (B) and (C)). Within M1, in the primary cohort, SN resting-state functional connectivity to the hip ROI was significantly lower than the shoulder ROI ($p = 0.0009$); similarly in the replication cohort, SN resting-state functional connectivity to the hip ROI was significantly lower than the shoulder ROI ($p < 0.0001$). Within S1, in the primary cohort, SN functional connectivity the index finger ROI was significantly lower than both the shoulder and hip ROIs ($p < 0.0001$; $p < 0.0001$ respectively); similarly in the replication cohort, the index finger ROI was significantly lower than both shoulder and hip ROIs ($p = 0.003$; $p = 0.002$ respectively). Inter-individual differences of motor and sensory circuit locations may explain some variability observed in SN-S1/M1 resting-state functional connectivity captured in the ROI analysis. We further explored the potential heterogeneities in SN-S1/M1 resting-state functional connectivity with a ROI free approach using a flatmap to explore changes in connectivity across the entire sensorimotor cortex.

3.5.   SN functional connectivity across S1/M1 surface

The spatial map of SN resting-state functional connectivity across the entire flattened cortical surface of S1/M1 showed relative peaks and minima in SN-S1/M1 resting-state functional connectivity consistent with the ROI analysis (Fig. 3). Relative differences in SN-S1/M1 resting-state functional connectivity were preserved from a map of the fiducial surface (Fig. 3 (A)), on an inflated surface (Fig. 3 (B)) and flattened surface (Fig. 3 (C)) of the cortex. It became clear inspecting flattened maps that the heterogeneity in SN-S1/M1 resting-state functional connectivity observed in the ROI analysis was part of a broader pattern of heterogeneity across S1/M1. In the primary cohort, local peaks and minima identified in the ROI analysis were seen on the full cortical map, but additional unidentified local peaks were present in lateral areas and ventromedial areas of both S1 and M1 (Fig. 3 (D)). Similar local minima and maxima were observed in SN resting-state functional connectivity across the cortical surface of M1 and S1 within the replication cohort (Fig. 3 (E)).

To explore the dependence of the SN-S1/M1 resting-state functional connectivity on distance from key SN brain regions, we further explored the results on the flattened map. Peak SN resting-state functional connectivity in the anterior insula and anterior cingulate cortex were found at ($-40,10, -1$) mm and ($-1,6,38$) mm expressed in MNI (x,y,z) standard space. The distance between the SN hubs and M1/S1 did not solely explain heterogeneity of the SN-M1/S1 resting-state functional connectivity (Fig. 4).

4.   Discussion

Sensorimotor and salience networks are known to function as distinct resting-state networks (Uddin et al., 2019). These large-scale networks are defined based both on co-activation of these brain regions during a range of relevant tasks, and the temporal correspondence of the same regions even at rest (for summary Uddin et al., 2019). While the sensorimotor and salience networks are understood to interact (Chang et al., 2012; Nomi et al., 2016; Uddin,

2015), the novelty of this study highlights the somatotopic dependence of their interaction even in healthy pain-free individuals. Specifically, we identified stronger SN-S1/M1 resting-state functional connectivity within the somatotopic representation of proximal body regions (trunk/face), compared to distal body regions (upper/lower limbs). Identification of non-homogenous SN-S1/M1 resting-state functional connectivity is especially meaningful as this resting-state feature has been associated with the signature of persistent pain conditions (Kim et al., 2019; Kutch et al., 2017).

Survival is contingent on the ability to rapidly assess incoming sensory information, to classify that information as relevant or irrelevant, and to initiate appropriate motor responses to mitigate threats. The SN is thought to fulfill the role of filtering the stream of sensory information and influencing the motor system (Uddin, 2015) through intercommunication among distributed brain regions including the anterior insula, anterior cingulate, thalamus, and amygdala (Seeley et al., 2007; Uddin, 2015).

The role of the SN describes a top-down mechanism used to modulate sensory experiences such as pain sensitivity and threat awareness. In this study, we interpret stronger SN-S1/M1 resting-state functional connectivity as a state of increased reliance of 'threat assessment' for specific body regions. General observations of human behavior support the theory that a "threat detection" system would prioritize core body regions, and are consistent with the general heterogeneous pattern of SN-S1/M1 resting-state functional connectivity strength that we observed across trunk, neck, and head somatotopy in S1/M1. Specifically, sensitivity to noxious stimuli is known to be higher in certain body areas compared to others, with generally lower sensitivity in the limbs (Defrin et al., 2006; Stevens et al., 1974). Furthermore, during protective motor behavior, limbs are often rapidly mobilized to protect trunk, neck, and head regions from impacts (Carlsöö and Johansson, 1962; Feldman and Robinovitch, 2007; Hsiao and Robinovitch, 1997; White et al., 1993). Interpretation of negative connectivity patterns identified between SN and S1/M1 in the limb somatotopic regions, while less prevalent in the literature, may reflect an inhibitory interaction between brain regions (Gee et al., 2013), or a time delayed excitatory interaction (Chen et al., 2011). While it's unclear the underlying mechanism of negative connectivity, a mutual inhibitory interaction could suggest a possible avenue to modulate salience network activity in individuals with chronic pain using stimulation points in sensorimotor cortex, a previously reported successful stimulation site (Quintero, 2013).

We must also acknowledge alternative hypotheses to explain the heterogeneities in SN-S1/M1 resting-state functional connectivity. Alternative hypothesis 1: the overall SN-S1/M1 resting-state functional connectivity strength may have been driven by the size of a body site's representative area in sensorimotor cortex. Body regions prioritized for fine motor control and touch perception (e.g. face, hand) have large representative areas (Penfield and Boldrey, 1937); however, evidence suggests anatomical connections between sensorimotor cortex and other brain regions, while somatotopically distinct are not scaled based on body region (Huffman and Krubitzer, 2001; Krubitzer and Kaas, 1990). Further, contradictory SN resting-state functional connectivity patterns in the hand and face regions suggest the size of the representational area alone does not dictate the SN-S1/M1 resting-state functional connectivity strength. Alternative hypothesis 2: heterogeneities in SN-S1/M1 resting-state

functional connectivity across sensorimotor cortex may have been driven by the proximity of sensorimotor regions to hubs within SN such as the anterior insula or anterior cingulate cortex. Functional connectivity can depend on spatial distance, with stronger short-range connections compared to long-range connections (e.g. Salvador et al., 2005) making this phenomenon important to quantify within this study. An analysis of SN-S1/M1 resting-state functional connectivity as a function of distance from both the anterior insula and anterior cingulate cortex showed while there are local peaks in connectivity within S1/M1 near the two critical hubs of SN, the heterogeneities of interest between the shoulder, finger, and gluteal ROIs are not explained by geometric distance to SN hubs (Fig. 4). To confirm our interpretation of SN-S1/M1 resting-state functional connectivity as a behavioral feature, future work must establish a link between threat-based sensory sensitivity or motor responsiveness to SN-S1/M1 resting-state functional connectivity, but our results clearly suggest future studies in this direction.

Extensive evidence suggests the sensorimotor system, in a somatotopically distinct way, is integrally tied to the representation of centralized pain. Changes in SN-S1/M1 resting-state functional connectivity have been shown in a number of chronic pain conditions including chronic pelvic pain, fibromyalgia, and chronic low-back pain (Kim et al., 2019; Kutch et al., 2017). In addition, the retention of motor cortical representation and its connectivity to widespread brain networks in the hand motor area of M1 has been linked with higher perception of phantom limb pain in individuals with an upper limb amputation (Makin et al., 2015; Makin et al., 2013). Modulation of pain perception through emotional, affective, and attentional changes has previously provided clear evidence of the involvement of cortical structures in altering an individual's perceived pain (Bantick et al., 2002; Tracey and Mantyh, 2007; Wiech et al., 2010). However, there is comparatively little evidence exploring how somatotopic-dependent interactions between key pain processing regions such as S1/M1, S2 and insula may also result in altered pain perception through a top-down driven approach (Baumgärtner et al., 2010). From an epidemiological perspective, chronic pain is not uniformly distributed across the body surface, but instead tends to cluster in particular regions including the low back, head, neck, abdomen, and genitals (Maixner et al., 2016; Statistics, 2017; Von Korff et al., 1988). We hope to explore in future studies if specific subdivisions within the salience network play unique or driving roles in heightened functional connectivity to S1/M1 increasing our understanding of key brain regions involved in body representation and its relevance to centralized pain.

We propose that heterogeneity in SN-S1/M1 resting-state functional connectivity found in this study may partially explain susceptibility of different body regions to chronic pain development through two mechanisms. First, body regions with intrinsically greater SN-S1/M1 functional connectivity may react more intensely when exposed to injury, resulting in a longer-lasting state of increased threat assessment and vigilance. For example, chronic pain may emerge from whiplash injury in a motor vehicle accident (McLean et al., 2005). Second, top-down systemic stressors that increase engagement of the salience system might be expected to preferentially activate areas of S1/M1 with pre-existing greater functional connectivity. For example, the role of stress has been described in chronic pelvic pain conditions that are not associated with co-morbid pain in the extremities, including the hands (Harte et al., 2019; Kutch et al., 2015; Naliboff et al., 2015; Nickel et al., 2010;

Rothrock et al., 2001). Further research is needed to test whether SN-S1/M1 resting-state functional connectivity can predict chronic pain development in specific body regions.

While this study focused on the somatotopic organization of SN resting-state functional connectivity as a feature important to map, dysregulation of other widespread brain networks such as default mode network have also been implicated in chronic pain. Altered default mode network activity has been found in patients with chronic pain, in association the presence of pain catastrophizing, the perception of pain severity, and aberrant signaling of pain perception when no peripheral threat is evident (Kim et al., 2019; Loggia et al., 2013; Makin et al., 2015), as well as in co-morbid mental health condition such as anxiety and depression (Coutinho et al., 2016; Whitfield-Gabrieli and Ford, 2012). Future studies evaluating widespread network interaction should consider how interaction with somatotopically meaningful regions in S1/M1 may provide critical insight into the role of the body in central processing networks. Sensorimotor/salience links in pain may be only one example of much broader class of neural processes that use the somatosensory cortex and SN regions to monitor, predict, and control body state.

Supplementary Material

Refer to Web version on PubMed Central for supplementary material.

Acknowledgments

References

Alger JR, Ellingson BM, Ashe-McNalley C, Woodworth DC, Labus JS, Farmer M, Huang L, Apkarian AV, Johnson KA, Mackey SC, 2016. Multisite, multimodal neuroimaging of chronic urological pelvic pain: methodology of the MAPP research network. NeuroImage: Clin12, 65–77. [PubMed: 27408791]

Apkarian AV, Bushnell MC, Treede RD, Zubieta JK, 2005. Human brain mechanisms of pain perception and regulation in health and disease. Eur. J. Pain9, 463–463. [PubMed: 15979027]

Asavasopon S, Rana M, Kirages DJ, Yani MS, Fisher BE, Hwang DH, Lohman EB, Berk LS, Kutch JJ, 2014. Cortical activation associated with muscle synergies of the human male pelvic floor. J. Neurosci34, 13811–13818. [PubMed: 25297107]

Baliki MN, Petre B, Torbey S, Herrmann KM, Huang L, Schnitzer TJ, Fields HL, Apkarian AV, 2012. Corticostriatal functional connectivity predicts transition to chronic back pain. Nat. Neurosci15, 1117. [PubMed: 22751038]

Banker L, Tadi P, 2019. Neuroanatomy, Precentral Gyrus. StatPearls[Internet].StatPearls Publishing.

Bantick SJ, Wise RG, Ploghaus A, Clare S, Smith SM, Tracey I, 2002. Imaging how attention modulates pain in humans using functional MRI. Brain125, 310–319. [PubMed: 11844731]

Bastin J, Deman P, David O, Gueguen M, Benis D, Minotti L, Hoffman D, Com-brisson E, Kujala J, Perrone-Bertolotti M, 2016. Direct recordings from human anterior insula reveal its leading role within the error-monitoring network. Cereb. Cortexbhv352.

Baumgärtner U, Iannetti GD, Zambreanu L, Stoeter P, Treede R-D, Tracey I, 2010. Multiple somatotopic representations of heat and mechanical pain in the operculo-insular cortex: a high-resolution fMRI study. J. Neurophysiol104, 2863–2872. [PubMed: 20739597]

Beckmann CF, Mackay CE, Filippini N, Smith SM, 2009. Group comparison of resting-state FMRI data using multi-subject ICA and dual regression. Neuroimage47, S148.

Bingel U, Tracey I, 2008. Imaging CNS modulation of pain in humans. Physiology23, 371–380. [PubMed: 19074744]

Biswal BB, Mennes M, Zuo X-N, Gohel S, Kelly C, Smith SM, Beckmann CF, Adelstein JS, Buckner RL, Colcombe S, 2010. Toward discovery science of human brain function. Proc. Natl. Acad. Sci107, 4734–4739. [PubMed: 20176931]

Caballero-Gaudes C, Reynolds RC, 2017. Methods for cleaning the BOLD fMRI signal. Neuroimage154, 128–149. [PubMed: 27956209]

Carlsöö S, Johansson O, 1962. Stabilization of and load on the elbow joint in some protective movements. Cells Tissues Organs48, 224–231.

Chang LJ, Yarkoni T, Khaw MW, Sanfey AG, 2012. Decoding the role of the insula in human cognition: functional parcellation and large-scale reverse inference. Cereb. Cortex23, 739–749. [PubMed: 22437053]

Chen G, Chen G, Xie C, Li S-J, 2011. Negative functional connectivity and its dependence on the shortest path length of positive network in the resting-state human brain. Brain Connect1, 195–206. [PubMed: 22433048]

Coutinho JF, Fernandesl SV, Soares JM, Maia L, Gonçalves ÓF, Sampaio A, 2016. Default mode network dissociation in depressive and anxiety states. Brain Imaging Behav10, 147–157. [PubMed: 25804311]

Craig A, 2011. Significance of the insula for the evolution of human awareness of feelings from the body. Ann. N.Y. Acad. Sci1225, 72–82. [PubMed: 21534994]

Damoiseaux JS, Beckmann C, Arigita ES, Barkhof F, Scheltens P, Stam C, Smith S, Rombouts S, 2007. Reduced resting-state brain activity in the "default network" in normal aging. Cereb. Cortex18, 1856–1864. [PubMed: 18063564]

Defrin R, Shachal-Shiffer M, Hadgadg M, Peretz C, 2006. Quantitative somatosensory testing of warm and heat-pain thresholds: the effect of body region and testing method. Clin. J. Pain22, 130–136. [PubMed: 16428946]

DiGuiseppi J, Tadi P, 2019. Neuroanatomy, Postcentral Gyrus. StatPearls[Internet].StatPearls Publishing.

Drysdale AT, Grosenick L, Downar J, Dunlop K, Mansouri F, Meng Y, Fetcho RN, Zebley B, Oathes DJ, Etkin A, 2017. Resting-state connectivity biomarkers define neurophysiological subtypes of depression. Nat. Med23, 28. [PubMed: 27918562]

Etkin A, Egner T, Peraza DM, Kandel ER, Hirsch J, 2006. Resolving emotional conflict: a role for the rostral anterior cingulate cortex in modulating activity in the amygdala. Neuron51, 871–882. [PubMed: 16982430]

Feldman F, Robinovitch SN, 2007. Reducing hip fracture risk during sideways falls: evidence in young adults of the protective effects of impact to the hands and stepping. J. Biomech40, 2612–2618. [PubMed: 17395188]

Filippini N, MacIntosh BJ, Hough MG, Goodwin GM, Frisoni GB, Smith SM, Matthews PM, Beckmann CF, Mackay CE, 2009. Distinct patterns of brain activity in young carriers of the APOE-ε4 allele. Proc. Natl. Acad. Sci106, 7209–7214. [PubMed: 19357304]

Gao JS, Huth AG, Lescroart MD, Gallant JL, 2015. Pycortex: an interactive surface visualizer for fMRI. Front. Neuroinform9, 23. [PubMed: 26483666]

Gee DG, Humphreys KL, Flannery J, Goff B, Telzer EH, Shapiro M, Hare TA, Bookheimer SY, Tottenham N, 2013. A developmental shift from positive to negative connectivity in human amygdala–prefrontal circuitry. J. Neurosci33, 4584–4593. [PubMed: 23467374]

Harte SE, Schrepf A, Gallop R, Kruger GH, Lai HHH, Sutcliffe S, Halvorson M, Ichesco E, Naliboff BD, Afari N, 2019. Quantitative assessment of nonpelvic pressure pain sensitivity in urologic chronic pelvic pain syndrome: a MAPP research network study. Pain160, 1270–1280. [PubMed: 31050659]

Hsiao ET, Robinovitch SN, 1997. Common protective movements govern unexpected falls from standing height. J. Biomech31, 1–9.

Huffman KJ, Krubitzer L, 2001. Area 3a: topographic organization and cortical connections in marmoset monkeys. Cereb. Cortex11, 849–867. [PubMed: 11532890]

Ingalhalikar M, Smith A, Parker D, Satterthwaite TD, Elliott MA, Ruparel K, Hakonarson H, Gur RE, Gur RC, Verma R, 2014. Sex differences in the structural connectome of the human brain. Proc. Natl. Acad. Sci111, 823–828. [PubMed: 24297904]

Kairys AE, Schmidt-Wilcke T, Puiu T, Ichesco E, Labus JS, Martucci K, Farmer MA, Ness TJ, Deutsch G, Mayer EA, 2015. Increased brain gray matter in the primary somatosensory cortex is associated with increased pain and mood disturbance in patients with interstitial cystitis/painful bladder syndrome. J. Urol193, 131–137. [PubMed: 25132239]

Kilpatrick LA, Zald DH, Pardo JV, Cahill L, 2006. Sex-related differences in amygdala functional connectivity during resting conditions. Neuroimage30, 452–461. [PubMed: 16326115]

Kim J, Mawla I, Kong J, Lee J, Gerber J, Ortiz A, Kim H, Chan S-T, Loggia ML, Wasan AD, 2019. Somatotopically specific primary somatosensory connectivity to salience and default mode networks encodes clinical pain. Pain160, 1594–1605. [PubMed: 30839429]

Krubitzer LA, Kaas JH, 1990. The organization and connections of somatosensory cortex in marmosets. J. Neurosci10, 952–974. [PubMed: 2108231]

Kutch JJ, Ichesco E, Hampson JP, Labus JS, Farmer MA, Martucci KT, Ness TJ, Deutsch G, Apkarian AV, Mackey SC, 2017. Brain signature and functional impact of centralized pain: a multidisciplinary approach to the study of chronic pelvic pain (MAPP) network study. Pain158, 1979–1991. [PubMed: 28692006]

Kutch JJ, Yani MS, Asavasopon S, Kirages DJ, Rana M, Cosand L, Labus JS, Kilpatrick LA, Ashe-McNalley C, Farmer MA, 2015. Altered resting state neuro-motor connectivity in men with chronic prostatitis/chronic pelvic pain syndrome: a MAPP: research network neuroimaging study. NeuroImage: Clin8, 493–502. [PubMed: 26106574]

Laird AR, Fox PM, Eickhoff SB, Turner JA, Ray KL, McKay DR, Glahn DC, Beckmann CF, Smith SM, Fox PT, 2011. Behavioral interpretations of intrinsic connectivity networks. J. Cogn. Neurosci23, 4022–4037. [PubMed: 21671731]

Loggia ML, Kim J, Gollub RL, Vangel MG, Kirsch I, Kong J, Wasan AD, Na-padow V, 2013. Default mode network connectivity encodes clinical pain: an arterial spin labeling study. PAIN®154, 24–33. [PubMed: 23111164]

Maixner W, Fillingim RB, Williams DA, Smith SB, Slade GD, 2016. Overlapping chronic pain conditions: implications for diagnosis and classification. J. Pain17, T93–T107. [PubMed: 27586833]

Makin TR, Filippini N, Duff EP, Slater DH, Tracey I, Johansen-Berg H, 2015. Network-level reorganisation of functional connectivity following arm amputation. Neuroimage114, 217–225. [PubMed: 25776216]

Makin TR, Scholz J, Filippini N, Slater DH, Tracey I, Johansen-Berg H, 2013. Phantom pain is associated with preserved structure and function in the former hand area. Nat. Commun4, 1570. [PubMed: 23463013]

Makris N, Goldstein JM, Kennedy D, Hodge SM, Caviness VS, Faraone SV, Tsuang MT, Seidman LJ, 2006. Decreased volume of left and total anterior insular lobule in schizophrenia. Schizophr. Res83, 155–171. [PubMed: 16448806]

McLean SA, Clauw DJ, Abelson JL, Liberzon I, 2005. The development of persistent pain and psychological morbidity after motor vehicle collision: integrating the potential role of stress response systems into a biopsychosocial model. Psychosom. Med67, 783–790. [PubMed: 16204439]

Naliboff BD, Stephens AJ, Afari N, Lai H, Krieger JN, Hong B, Lutgendorf S, Strachan E, Williams D, Network MR, 2015. Widespread psychosocial difficulties in men and women with urologic chronic pelvic pain syndromes: case-control findings from the multidisciplinary approach to the study of chronic pelvic pain research network. Urology85, 1319–1327. [PubMed: 26099876]

Nickel JC, Tripp DA, Pontari M, Moldwin R, Mayer R, Carr LK, Doggweiler R, Yang CC, Mishra N, Nordling J, 2010. Psychosocial phenotyping in women with interstitial cystitis/painful bladder syndrome: a case control study. J. Urol183, 167–172. [PubMed: 19913812]

Noble S, Scheinost D, Finn ES, Shen X, Papademetris X, McEwen SC, Bear-den CE, Addington J, Goodyear B, Cadenhead KS, 2017. Multisite reliability of MR-based functional connectivity. Neuroimage146, 959–970. [PubMed: 27746386]

Nomi JS, Farrant K, Damaraju E, Rachakonda S, Calhoun VD, Uddin LQ, 2016. Dynamic functional network connectivity reveals unique and overlapping profiles of insula subdivisions. Hum. Brain Mapp37, 1770–1787. [PubMed: 26880689]

Ogino Y, Nemoto H, Goto F, 2005. Somatotopy in human primary somatosensory cortex in pain system. Anesthesiol.: J. Am. Soc. Anesthesiol103, 821–827.

Penfield W, Boldrey E, 1937. Somatic motor and sensory representation in the cerebral cortex of man as studied by electrical stimulation. Brain60, 389–443.

Poldrack RA, Mumford JA, Nichols TE, 2011. Handbook of Functional MRI Data AnalysisCambridge University Press.

Quintero GC, 2013. Advances in cortical modulation of pain. J. Pain Res6, 713. [PubMed: 24092997]

Rana M, Yani MS, Asavasopon S, Fisher BE, Kutch JJ, 2015. Brain connectivity associated with muscle synergies in humans. J. Neurosci35, 14708–14716. [PubMed: 26538643]

Rothrock NE, Lutgendorf SK, Kreder KJ, Ratliff T, Zimmerman B, 2001. Stress and symptoms in patients with interstitial cystitis: a life stress model. Urology57, 422–427. [PubMed: 11248609]

Ruben J, Schwiemann J, Deuchert M, Meyer R, Krause T, Curio G, Villringer K, Kurth R, Villringer A, 2001. Somatotopic organization of human secondary somatosensory cortex. Cereb. Cortex11, 463–473. [PubMed: 11313298]

Salvador R, Suckling J, Coleman MR, Pickard JD, Menon D, Bullmore E, 2005. Neurophysiological architecture of functional magnetic resonance images of human brain. Cereb. Cortex15, 1332–1342. [PubMed: 15635061]

Seeley WW, Menon V, Schatzberg AF, Keller J, Glover GH, Kenna H, Reiss AL, Greicius MD, 2007. Dissociable intrinsic connectivity networks for salience processing and executive control. J. Neurosci27, 2349–2356. [PubMed: 17329432]

Singer T, Seymour B, O'doherty J, Kaube H, Dolan RJ, Frith CD, 2004. Empathy for pain involves the affective but not sensory components of pain. Science303, 1157–1162. [PubMed: 14976305]

Statistics, N.C.f.H., 2017. Health, United States, 2016, with Chartbook on Long-term Trends in HealthGovernment Printing Office.

Stevens JC, Marks LE, Simonson DC, 1974. Regional sensitivity and spatial summation in the warmth sense. Physiol. Behav13, 825–836. [PubMed: 4445288]

Tracey I, Mantyh PW, 2007. The cerebral signature for pain perception and its modulation. Neuron55, 377–391. [PubMed: 17678852]

Uddin LQ, 2015. Salience processing and insular cortical function and dysfunction. Nat. Rev. Neurosci16, 55. [PubMed: 25406711]

Uddin LQ, 2016. Salience Network of the Human BrainAcademic Press.

Uddin LQ, Yeo BT, Spreng RN, 2019. Towards a universal taxonomy of macro-scale functional human brain networks. Brain Topogr1–17.

Von Korff M, Dworkin SF, Le Resche L, Kruger A, 1988. An epidemiologic comparison of pain complaints. Pain32, 173–183. [PubMed: 3362555]

Wager TD, Atlas LY, Lindquist MA, Roy M, Woo C-W, Kross E, 2013. An fMRI-based neurologic signature of physical pain. N. Engl. J. Med368, 1388–1397. [PubMed: 23574118]

White B, Firth J, Rowles J, 1993. The effects of brace position on injuries sustained in the M1 Boeing 737/400 disaster, January 1989. NLDB Study Group. Aviat. Space Environ. Med64, 103–109. [PubMed: 8431182]

Whitfield-Gabrieli S, Ford JM, 2012. Default mode network activity and connectivity in psychopathology. Annu. Rev. Clin. Psychol8, 49–76. [PubMed: 22224834]

Wiech K, Lin C-S, Brodersen KH, Bingel U, Ploner M, Tracey I, 2010. Anterior insula integrates information about salience into perceptual decisions about pain. J. Neurosci30, 16324–16331. [PubMed: 21123578]

Woolrich MW, Jbabdi S, Patenaude B, Chappell M, Makni S, Behrens T, Beckmann C, Jenkinson M, Smith SM, 2009. Bayesian analysis of neuroimaging data in FSL. Neuroimage45, S173–S186. [PubMed: 19059349]

Wu Q, Inman RD, Davis KD, 2013. Neuropathic pain in ankylosing spondylitis: a psychophysics and brain imaging study. Arthr. Rheum65, 1494–1503. [PubMed: 23460087]

Yani MS, Wondolowski JH, Eckel SP, Kulig K, Fisher BE, Gordon JE, Kutch JJ, 2018. Distributed representation of pelvic floor muscles in human motor cortex. Sci. Rep8, 7213. [PubMed: 29740105]
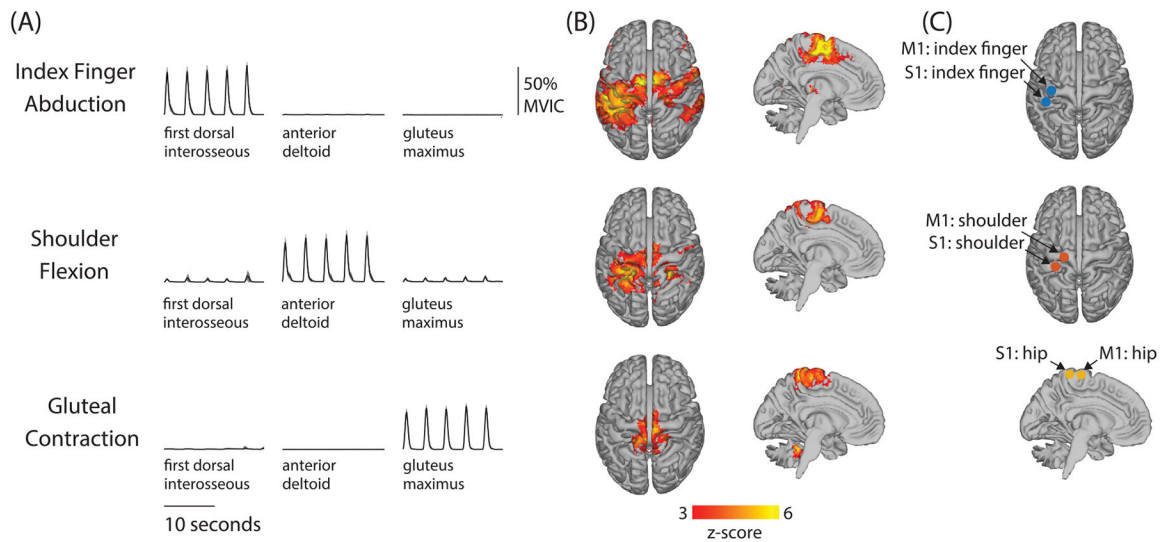
Fig. 1.
Muscle activity and brain activity measured during controlled isometric motor tasks. A block paradigm of rest-active-rest task with 6 active blocks were performed, and muscle activity was evoked in a pulse active fashion. Participants were asked to perform an active isometric contraction every 4 s during the active period. Panel (A) shows electromyographic activity during one active block where 4 s pulse active isometric contractions are evident. Three motor tasks were performed including index finger abduction (row 1), shoulder flexion (row 2), and gluteal contraction where participants were instructed to "squeeze" their gluteal muscles (row 3). Electromyography was collected from three instrumented muscles active during the motor tasks including first dorsal interosseous active during finger abduction, anterior deltoid active during shoulder flexion, and gluteus maximus active during gluteal contraction. Average muscle activity across all participants (black) and standard error (gray) is shown for a contraction level of 30% maximum voluntary isometric contraction (MVIC) for each motor task. Panel (B) shows brain regions where brain activity was significantly elevated during active periods compared to rest within the block paradigm motor tasks shown in a superior view of the cortical surface and sagittal view from the midline. Panel (C) shows calculated regions-of-interest for each muscle within primary motor cortex (M1) and primary sensory cortex (S1).
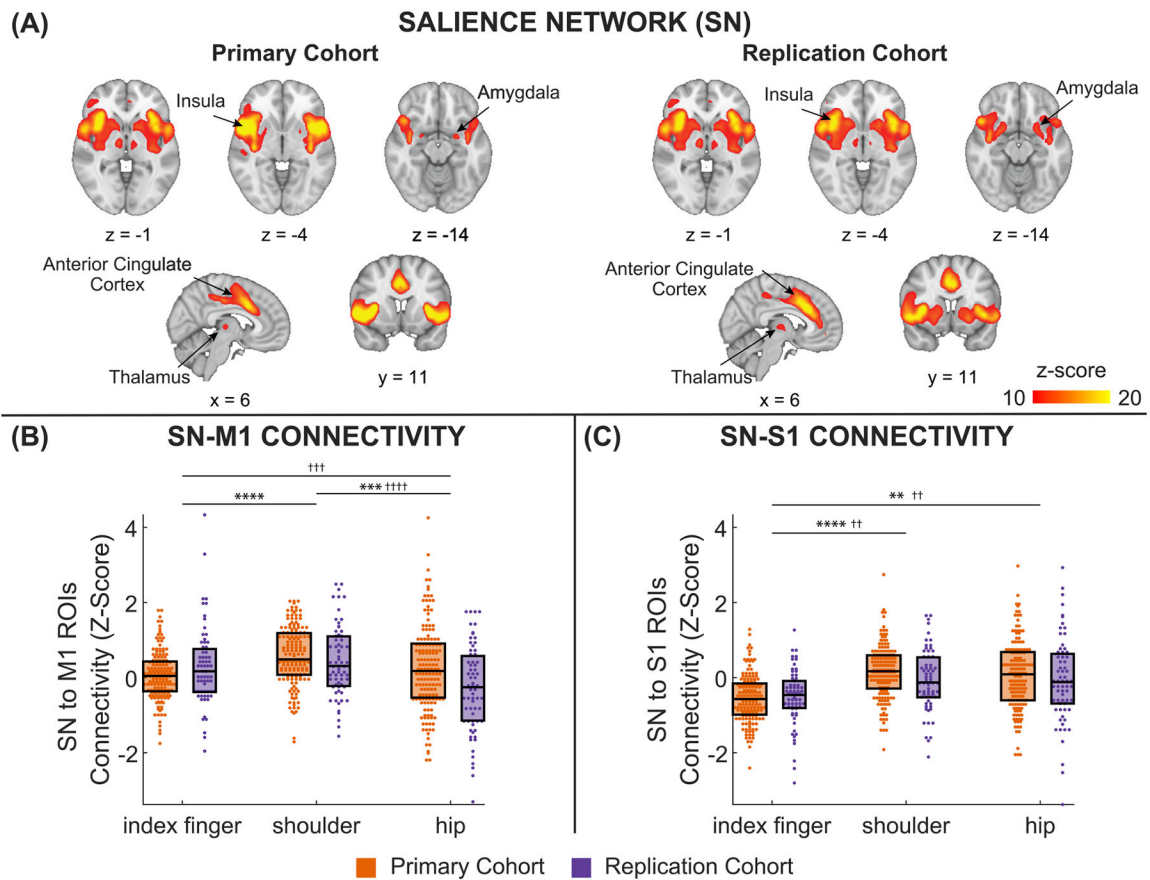
Fig. 2.

Salience network (SN) connectivity to primary sensorimotor cortex. Panel (A) primary cohort SN group map indicating spatial regions strongly connected. Primary nodes in the SN are indicated including bilateral insula, thalamus, and anterior cingulate cortex. Panel (B) shows average SN resting-state functional connectivity to M1 regions-of-interest for all participants in the primary cohort (orange) and replication cohort (purple). Panel (B) shows average SN resting-state functional connectivity to S1 regions-of-interest for all participants in the primary cohort (orange) and replication cohort (purple). SN resting-state functional connectivity between regions-of-interest were significantly different within both M1 and S1 as indicated (primary cohort: $p < 0.01$ **, $p < 0.001$ ***, $p < 0.0001$ ****; replication cohort: $p < 0.01$ ††, $p < 0.001$ †††, $p < 0.0001$ ††††). Significant differences validated in both groups are indicated with both "∗ †".
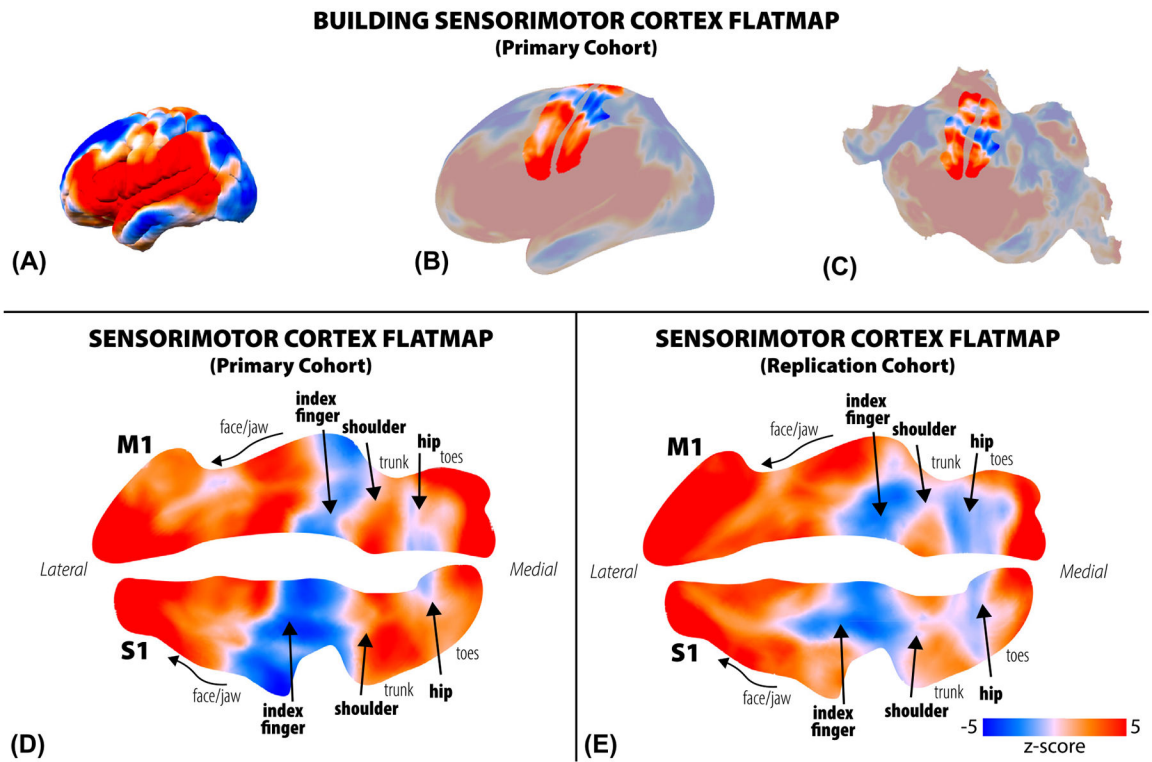
Fig. 3.

Salience network (SN) resting-state functional connectivity across the sensorimotor cortex (S1/M1). Development of the flatmap representation of the SN strength within the primary cohort is shown step by step as first shown (A) on the cortical fiducial surface; (B) on the inflated surface of the cortex, and (C) laid flat showing the entire cortical surface. The precentral and postcentral gyri are highlighted in the inflated (B) and flattened (C) cortical surface. Precentral (M1) and postcentral (S1) gyri are then shown independently (D) and rotated to show the medial wall on the right and lateral gyri surface on the left and annotated with ROIs from current analysis. SN resting-state functional connectivity across the sensorimotor cortex within the replication cohort is also shown (E). Local peaks in connectivity are shown in red, and are present in far lateral cortical area, mid-cortex, and medial cortex in both cohorts. Local minima with low connectivity or anti-phase connectivity are shown as white and blue, respectively, and are present in regions classically identified to represent the upper extremities and lower extremities in both cohorts.
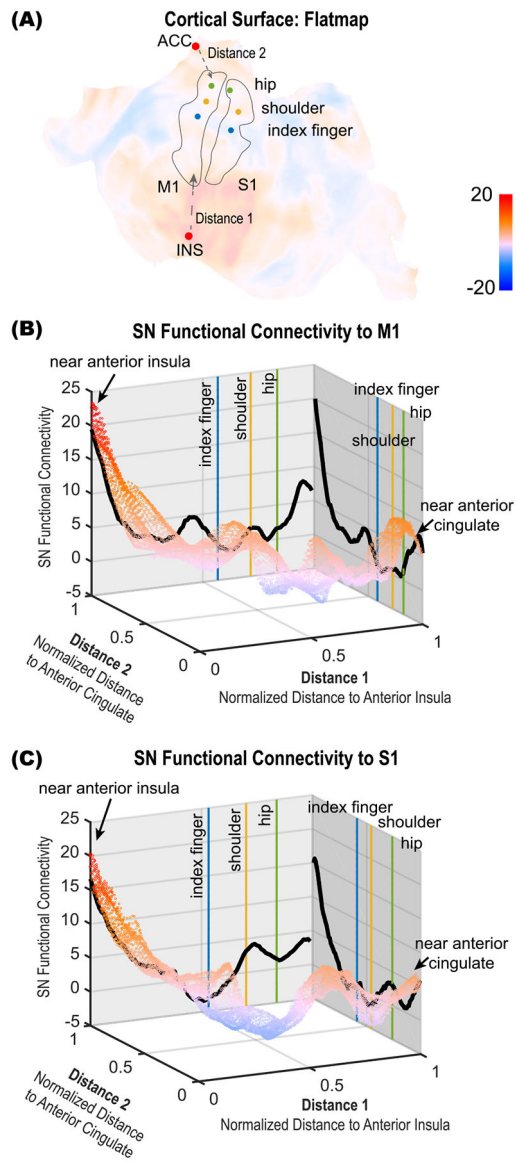
Fig. 4.

The relationship of salience network (SN) resting-state functional connectivity to the sensorimotor cortex is explored as a function of geodesic distance to SN hubs: anterior insula (INS) and anterior cingulate cortex (ACC). Cortical surface is defined by a flatmap surface model (Panel A). SN resting-state functional connectivity to primary motor (M1, Panel B) and to primary sensory (S1, Panel C) are shown for the entire cortical surface. Average SN functional connectivity as a function of normalized geodesic distance to Anterior Insula (Distance 1) and to Anterior Cingulate (Distance 2) are shown in black. Each task-defined region-of-interest is shown as anchors.

Table 1

Region-of-interest center of mass coordinates defined in MNI standard space (mm).

	Region-of-Interest Center		
Primary Motor Cortex	*X*	*Y*	*Z*
Index finger	−32	−14	51
Shoulder	−18	−22	63
Hip	1	−24	67
Primary Sensory Cortex			
Index finger	−38	−29	55
Shoulder	−30	−34	62
Hip	0	−39	68